MRS Advances
https://doi.org/10.1557/s43580-022-00215-4

ORIGINAL PAPER

Effect of thermal annealing on aggregation of a squaraine thin film

Zachary S. Walbrun[1] · Laura C. Leibfried[1] · Áine R. Hoban[1] · Brandon C. Rasmussen[1] · Tyler J. Wiegand[2] · Christopher J. Collison[2,3,4] · Cathy Y. Wong[1,5,6]

Received: 18 November 2021 / Accepted: 19 January 2022

Abstract
This study aimed to investigate the effects of thermal annealing on a film of squaraine (SQ) molecules in a polymethyl methacrylate (PMMA) matrix. Molecular aggregation is inferred from in situ absorption measurements, and excited state dynamics are measured using a spatially encoded transient absorption (TA) spectroscopy. TA spectra were well-replicated using a kinetic model that evolves as a function of annealing time and extent of aggregation. While linear absorbance spectra indicate that the SQ molecules are primarily uncoupled or weakly-coupled when initially deposited in a PMMA matrix, the kinetic model shows that some pi-stacked aggregates are already present. Excitons are funnelled by energy transfer to these aggregates in just a few picoseconds. The amount of pi-stacked aggregates increases during thermal annealing, further increasing the population of excitons that end up in these aggregates.

Introduction

Squaraine (SQ) dyes are donor–acceptor–donor (D–A–D) molecules consisting of an electron-accepting squarylium centre and two electron donating arms, each with a nitrogen centre [1, 2]. Excitons in these molecules have increased charge transfer character, which can aid in the charge separation process for photovoltaic applications [2, 3]. SQ molecules can be economically manufactured and solution-processed, and the resulting films can exhibit significant absorption of the solar spectrum. Their absorption spectrum can be chemically tuned by modifying the molecular structure or by influencing their molecular packing in films. A variety of molecular aggregates are typically produced when organic molecules are cast into films owing to weak intermolecular interactions [4, 5]. Kinetically trapped aggregates in unstable geometries lead to heterogeneity in the energetic landscape of a film and can act as carrier traps, inhibiting carrier mobility. The molecules in a film can rearrange and form larger, ordered, and more stable aggregates with solvent or thermal annealing. For the prototypical electron-donating polymer poly(3-hexylthiophene-2,5-diyl) (P3HT), for example, the carrier mobility increases from 10^{-11} to 10^{-8} m^2 V^{-1} s^{-1} when films are thermally annealed to form ordered crystalline domains [6]. However, larger aggregates that form during annealing can potentially also act as exciton traps [7], preventing excitons from migrating to an interface with an acceptor molecule. In some materials, there is a delicate balance between improved carrier mobility and creation of deleterious exciton traps that must be considered when annealing.

Molecular aggregates are typically categorized as either J- or H-aggregates [8]. J-aggregates are formed when electronic coupling is negative, typically when the transition dipole moments of the molecules are aligned in a head-to-tail fashion. Positive electronic coupling results in H-aggregation, typically when transition dipoles are positioned side-to-side. Intermolecular orientations that lie between these two extreme cases will also affect the

✉ Cathy Y. Wong
cwong3@uoregon.edu

1 Department of Chemistry and Biochemistry, University of Oregon, Eugene, OR 97403, USA

2 Department of Microsystems Engineering, College of Engineering, Rochester Institute of Technology, Rochester, NY 14623, USA

3 School of Chemistry and Materials Science, College of Science, Rochester Institute of Technology, Rochester, NY 14623, USA

4 Nanopower Research Laboratories, Rochester Institute of Technology, Rochester, NY 14623, USA

5 Oregon Center for Optical, Molecular, and Quantum Science, University of Oregon, Eugene, OR 97403, USA

6 Materials Science Institute, University of Oregon, Eugene, OR 97403, USA

Published online: 08 February 2022

electronic structure, and the 'type' of aggregate formed depends on the precise electronic coupling between molecules. For dimers of both types, the lowest excitonic state of each individual molecule will couple and split to yield two excitonic states in the molecular aggregate. For H-aggregates, the lower-energy exciton will have reduced oscillator strength while the oscillator strength of the higher energy exciton increases. This often results in a blue-shift of the absorption spectrum [9]. H-aggregation reliably causes a decreased ratio of the 0–0/0–1 vibronic absorption features. Conversely, J-aggregation leads to an increased 0–0/0–1 intensity ratio [10]. SQ molecules with linear side-chains off the donor atom exhibit H-aggregation in films, while SQ with branched side-chains inhibit pi–pi stacking and J-aggregates are formed instead [11].

Here we focus on a SQ molecule with linear side-chains, 2,4-bis(4-dihexylamino-2,6-dihydroxyphenyl) cyclobutene-1,3-dione [$DHSQ(OH)_2$]. In as-cast films of dilute $DHSQ(OH)_2$ in a polymer matrix of polymethyl methacrylate (PMMA), the $DHSQ(OH)_2$ molecules are primarily thought to exist as monomers, with varying orientation and distance between molecules. Calculations using a distribution of intermolecular distances and rotationally averaged intermolecular orientations have found that the intensity of the 0–1 vibronic absorption peak increases as the concentration of SQ increases [12]. Thus, the increased intensity of this feature has been ascribed to the presence of SQ molecules that are randomly oriented but close enough to each other to be weakly electronically coupled. Upon thermal annealing SQ H-aggregates form, which exhibit two absorption peaks at 560 nm and 648 nm, ascribed to transitions to excited states with less and more intermolecular charge transfer (CT) character, and thus stronger and weaker oscillator strength, respectively [13]. Here, we use these optical signatures of uncoupled, weakly coupled, and H-aggregated SQ molecules to quantify how thermal annealing affects the structure and dynamics of $DHSQ(OH)_2$ films using transient absorption (TA) spectroscopy.

Experimental details

A solution of 1.1 mg $DHSQ(OH)_2$ and 9.5 mg PMMA in 1 mL of chloroform was spin-cast onto a glass slide at 1500 RPM. As film absorbance does not change significantly between room temperature and 90 °C, we assert that annealing does not begin before 90 °C. The films were annealed from 90 to 140 °C, increasing by 10 °C every 10 min (Fig. 1a), on an electric hot plate with a slit in the middle, allowing light transmission for concurrent single-shot TA (SSTA) and absorbance measurements. The 42° pulse tilt used for SSTA measurements is shown in Fig. 1b with details provided elsewhere [14, 15]. The pump (419 nJ) and the probe (10 nJ) were spread over an overlap region of ~ 25 μm × 20 mm. SSTA and absorbance measurements were collected at 2 min and 58 min, which we refer to as pre- and post-annealing, respectively. Each SSTA measurement used a camera image size of 2560 × 180 pixels, and 3750 SSTA measurements were averaged over 60 s. On the time delay axis, two-pixel binning was used during data collection and a four-bin rolling average was applied during analysis.

Results and discussion

Absorbance spectra measured at 2 min and 58 min during annealing are shown in Fig. 1c, along with the pump spectrum. The height of the shoulder peak observed at 610 nm pre-annealing is attributed to weak Coulombic interactions between randomly oriented SQ molecules. Thermal annealing results in the formation of pi-stacked H-aggregates with absorbance at 560 nm and 648 nm.

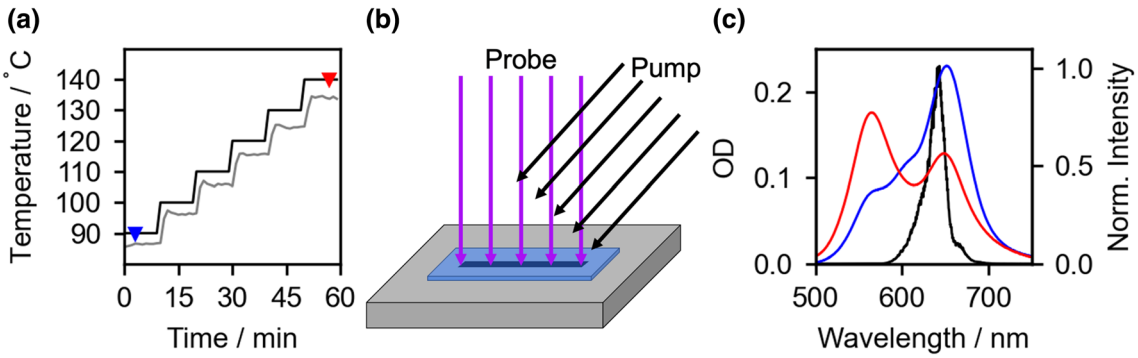

Fig. 1 **a** Temperature ramp of stage (black) and top surface of a glass slide (grey). Triangles indicate when spectroscopic measurements were conducted. **b** A film (blue) on a heated sample stage with slit that allows pump (black) and probe (purple) to pass. **c** Pump spectrum (black) overlaid with absorbance of $DHSQ(OH)_2$:PMMA film at 2 min (blue) and 58 min (red)

The SSTA spectra measured pre- and post-annealing are shown in Fig. 2. Before annealing, excitons are primarily photogenerated in monomers owing to their overlap with the pump spectrum. The pre-annealing spectrum exhibits a rapidly decaying ground state bleach (GSB) feature at 640 nm, corresponding to recovery of unexcited monomer. In the post-annealing spectrum, the features ascribed to both the uncoupled and weakly coupled monomer at 640 nm and 610 nm, respectively, have almost vanished and a strong GSB signal ascribed to H-aggregates is observed at 560 nm [13].

The rapid decay of signal at 640 nm and concomitant growth of the features at 610 nm and 560 nm suggests the migration of excitons from initially photoexcited uncoupled monomers to weakly-coupled molecules and H-aggregates [12]. Electronic coupling between randomly oriented SQ molecules results in the increased 0–1/0–0 peak ratio [9]. Stronger electronic coupling between pi-stacked SQ molecules with a smaller intermolecular distance [13] results in a blue-shifted absorption peak. In a similar SQ molecule (with butyl side chains) H-aggregates were found to have a lower energy excited state with substantial intermolecular CT character, owing to the proximity of the nitrogen atoms to the squarylium rings of neighbouring molecules in the aggregate. This type of CT state is mixed with the excitonic state, giving it enough oscillator strength to produce a peak at 648 nm in absorbance spectra, overlapping with the monomer peak [16]. Energy transfer is expected from the initially excited uncoupled monomers to weakly-coupled molecules and to pi-stacked H-aggregates. Exciton population in each of these SQ configurations will bleach the optical transitions observed in their linear absorbance spectra. The growth of these bleach features and the decay of the main monomer peak at 640 nm as a function of pump-probe delay time is apparent in the TA spectrum of the pre-annealed film (Fig. 2a). Growth of the H-aggregate and shoulder features is not observed in the SSTA spectrum of the post-annealed film (Fig. 2b). This film is expected to be comprised of almost entirely pi-stacked H-aggregates, and the laser excitation is resonant with their lower-energy CT state. Thus, the excitons can be directly photogenerated in H-aggregates in post-annealed films.

The observations described above motivate the kinetic model pictured in Fig. 3. Three separate models are used to describe the different film morphologies during thermal annealing. The first model represents regions of the film without pi-stacked H-aggregates and the last model describes regions of the film with only H-aggregates and without monomers. The second model describes film regions with a population of uncoupled monomers, weakly-coupled monomers, and pi-stacked H-aggregates in close enough proximity for energy transfer.

The model without pi-stacked H-aggregates, Fig. 3a, includes the excitonic state of SQ monomers that are uncoupled and weakly coupled to other monomers, S_{10}^{u} and S_{10}^{w}, respectively, and their ground states, S_{00}^{u} and S_{00}^{w}. Excitons can recombine from either excited state with rates of k_{1-0}^{u} and k_{1-0}^{w} for the uncoupled and weakly-coupled monomers, respectively, and energy can transfer from the uncoupled to the weakly-coupled monomers with a rate of k^{u-w}. The second model, Fig. 3b, duplicates the first model, but also includes the pi-stacked H-aggregate excited state, S_1^{π}, and ground state, S_0^{π}. The rate of energy transfer from monomers to pi-stacked H-aggregates is $k^{u-\pi}$. Reverse transitions were not necessary to adequately replicate the trends in the data, so these transitions were excluded to simplify the

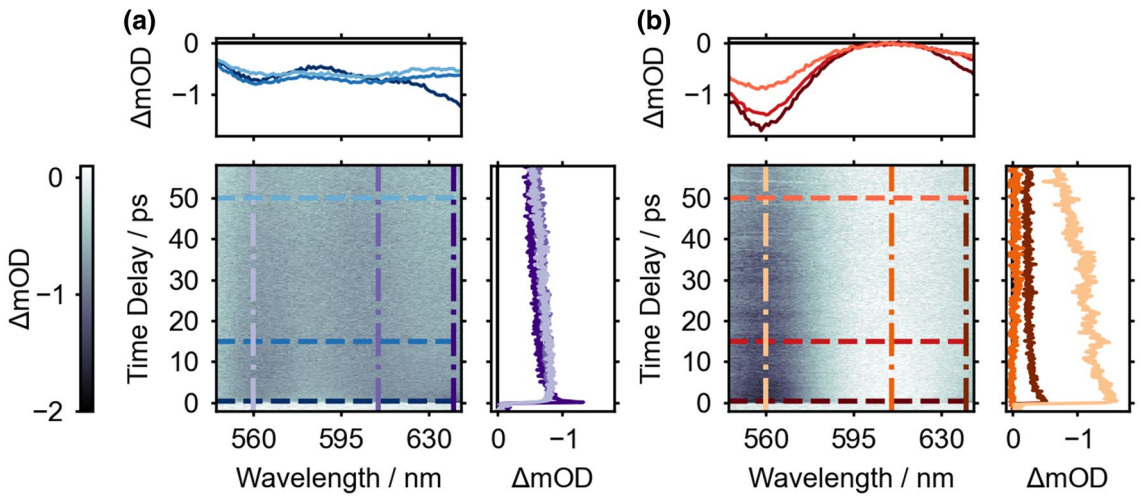

Fig. 2 SSTA measured at **a** 2 min and **b** 58 min. Above, spectral slices at pump-probe time delays of 0.2–0.5 ps, 14.5–15.5 ps, and 49.5–50.5 ps. On the right, transients at 560 nm, 610 nm, and 640 nm

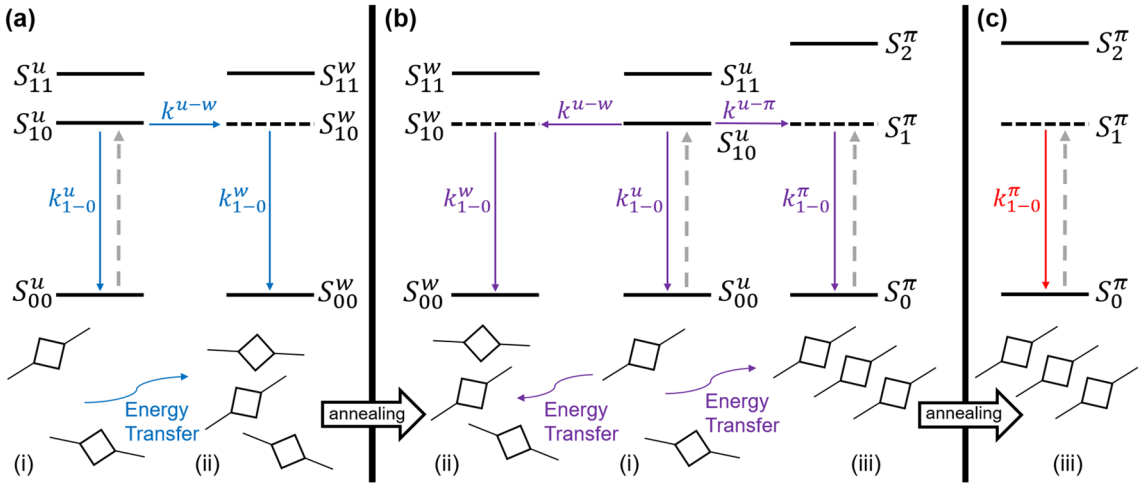

Fig. 3 The kinetic model for **a** uncoupled and weakly-coupled monomers, **b** uncoupled, weakly-coupled, and pi-stacked molecules, and **c** isolated pi-stacked molecules. States with lower oscillator strength shown in dashed lines. Cartoons illustrate the species present. Higher energy excited states that do not participate in the kinetic model but are bleached in the calculated TA spectra are also pictured. Model parameters reported in text. The grey dashed arrows indicate transitions that were excited by the 640 nm pump pulse

model. The third model, Fig. 3c, only considers pi-stacked H-aggregates. The S_1^π state, with a similar energy to that of the S_{10}^u state, has been attributed to an intermolecular CT state within the pi-stacked H-aggregate [16].

A weighted sum of the three models is used to simulate the population dynamics. The weights of the models were assigned based on three-Gaussian fits of the absorbance spectra. The fraction of pi-stacked molecules was estimated as the ratio of the height of the 560 nm peak compared to the maximal height of the feature, occurring at the latest time point where full aggregation was assumed. The weight of the first model was set as the fraction of molecules that are not pi-stacked. The fraction of the remaining molecules that were weakly coupled was determined by the height of the shoulder feature at 610 nm compared to its maximal height. The weight of the second model was set to be the fraction of weakly coupled molecules, with the weight of the third model being one minus the other two weights.

All features observed in the TA spectra are assumed to originate from GSB. All transitions shown in Fig. 3 as well as transitions from the respective ground states to the S_{11}^u, S_{11}^w, and S_2^π states are bleached. The intensity of the bleach is derived from the populations of each state and the peak ratios, discussed below. With the first and second model, the first vibronic state for the monomers is also bleached, which gives rise to the shoulder feature at 610 nm. In the second and third models, the H-aggregate absorbance feature at 560 nm is also bleached when there is excited H-aggregate population. Simulated TA spectra are calculated by using the populations of each electronic state from the kinetic model to weight the amplitude of Gaussian line shapes centred at the wavelengths of features in the linear absorbance spectrum. The population of S_{10}^u bleaches both the $S_{10}^u \leftarrow S_{00}^u$ and $S_{10}^w \leftarrow S_{00}^w$ transitions, so this population weights the amplitude of Gaussians centred at 640 nm and 610 nm. The relative intensity of these two features was assumed to be 1:0.2, estimated from the computations of [12]. Similarly, the population of S_{10}^w bleaches both the $S_{10}^u \leftarrow S_{00}^u$ and $S_{10}^w \leftarrow S_{00}^w$ transitions, so this population also weights the amplitude of Gaussians centred at 640 nm and 610 nm, this time with a relative intensity of 1:0.65 [12]. The population in S_1^π bleaches both the $S_{10}^u \leftarrow S_{00}^u$ and $S_1^\pi \leftarrow S_0^\pi$ transitions, so this population weights the amplitude of Gaussians centred at 640 nm and 560 nm, with relative intensities of 0.3:1, estimated from the absorption spectrum of the post-annealed film. The precise centre-wavelengths and broadening parameters were extracted from three-Gaussian fits of the absorbance spectra.

Figure 4a shows TA spectra averaged from 0.2–0.5 ps, 14.5–15.5 ps, and 49.5–50.5 ps for a $DHSQ(OH)_2$:PMMA film measured at 2 min and 58 min during thermal annealing. Figure 4b depicts transients simulated using the models described above at 0.3 ps, 15 ps, and 50 ps. A best-fit of the rates and relative weights of the three models has not yet been obtained, and the simulated spectra shown here are merely utilizing user-defined guesses. A time constant of 500 ps was selected for the transition anticipated to have lower oscillator strength ($S_{10}^w \leftarrow S_{00}^w$) and shorter time constants (60 ps and 40 ps) were assumed for the $S_1^\pi \leftarrow S_0^\pi$ and $S_{10}^u \leftarrow S_{00}^u$ transitions, respectively. Even without a best-fit, there is general agreement between the model and the experimental data. Increased signal intensity at 610 nm in the SSTA spectrum of the film pre-annealing is evidence of energy transfer from the excited uncoupled monomers to the

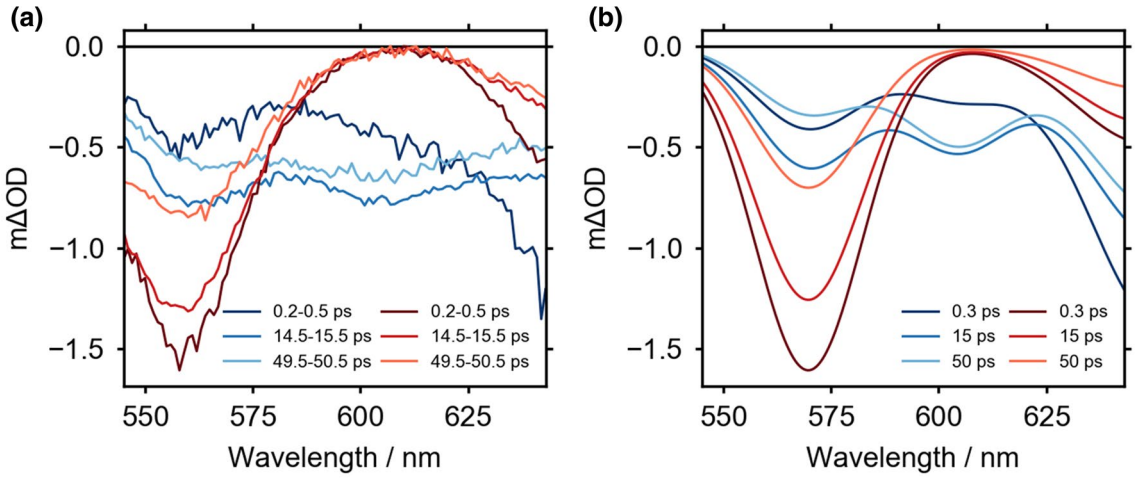

Fig. 4 **a** SSTA spectra measured at 2 min (pre-annealing, blue) and 58 min (post-annealing, red). **b** Simulated spectra at the same pump-probe time delays. The same parameters were used for shared transitions in multiple models: $\tau^{u}_{1-0} = 40$ ps, $\tau^{w}_{1-0} = 500$ ps, $\tau^{\pi}_{1-0} = 60$ ps, $\tau_{u-w} = 5$ ps, $\tau_{u-\pi} = 5$ ps. Weights of model 1:model 2:model 3 are 0.47:0.29:0.24 at 2 min and 0.00:0.30:0.70 at 58 min

weakly coupled monomers. Similarly, the 560 nm feature represents GSB of pi-stacked aggregates as a result of energy transfer from photoexcited monomer to the aggregates. The 5 ps value selected for τ_{u-w} and $\tau_{u-\pi}$ in our model is a reasonable rate for FRET between an organic donor–acceptor pair [17]. Post-annealing, the SSTA spectrum displays the bleach features associated with H-aggregates immediately after photoexcitation, suggesting that excitons are directly photogenerated in the pi-stacked H-aggregates in these films. Reasonable agreement between the experimental and simulated spectra was attained when assuming that the third model, with only pi-stacked H-aggregates, is dominant for the post-annealed film. However, inclusion of the second model is required to account for slower initial decay of the H-aggregate feature than would be expected for pure H-aggregates. Further refinement of the model and the identification of best-fit parameters may yield better agreement for the relative magnitudes of the three primary spectral features.

Conclusions

The trends in the dynamics of $DHSQ(OH)_2$:PMMA films before and after thermal annealing are well-replicated by a kinetic model that separately models isolated populations of monomers and H-aggregates and also models regions of film where these species are in close enough proximity to undergo energy transfer. The determination of best-fits will improve the agreement and may potentially yield additional insights. The measurement and analysis of transients measured during thermal annealing will enable further model refinement and may yield information on how the populations of uncoupled, weakly-coupled, and pi-stacked molecules, and the energy transfer rates between them, change as a function of thermal annealing time. These energy transfer rates can then be correlated to structure, as ascertained from the linear absorption spectra. This may lead to insights regarding the fate of photoexcited species in these films, which would have an impact on their potential for use in photovoltaic devices.

Acknowledgments The authors acknowledge Michael L. Crawford for assistance with kinetic modelling. This material is based upon work supported by the National Science Foundation under Grant No. 1752129.

Data availability The datasets generated during and/or analysed during the current study are available from the corresponding author on reasonable request.

Declarations

Conflict of interest On behalf of all authors, the corresponding author states that there is no conflict of interest.

References

1. Y. Diao, L. Shaw, Z. Bao, S.C.B. Mannsfeld, Energy Environ. Sci. **7**, 2145–2159 (2014)
2. M. Gsänger, D. Bialas, L. Huang, M. Stolte, F. Würthner, Adv. Mater. **28**, 3615–3645 (2016)
3. D. Zhang, M. Heeney, Asian J. Org. Chem. **9**, 1251–1251 (2020)
4. M.T. Seifrid, S.D. Oosterhout, M.F. Toney, G.C. Bazan, ACS Omega **3**, 10198–10204 (2018)
5. J. Rivnay, R. Steyrleuthner, L.H. Jimison, A. Casadei, Z. Chen, M.F. Toney, A. Facchetti, D. Neher, A. Salleo, Macromolecules **44**, 5246–5255 (2011)

6. R.A. Marsh, J.M. Hodgkiss, S. Albert-Seifried, R.H. Friend, Nano Lett. **10**, 923–930 (2010)
7. A. Serbenta, O.V. Kozlov, G. Portale, P.H.M. van Loosdrecht, M.S. Pshenichnikov, Sci. Rep. **6**, 36236 (2016)
8. M. Kasha, Radiat. Res. **20**, 55–70 (1963)
9. C. Zheng, C. Zhong, C.J. Collison, F.C. Spano, J. Phys. Chem. C **123**, 3203–3215 (2019)
10. F.C. Spano, Acc. Chem. Res. **43**, 429–439 (2010)
11. G. Chen, H. Sasabe, Y. Sasaki, H. Katagiri, X.-F. Wang, T. Sano, Z. Hong, Y. Yang, J. Kido, Chem. Mater. **26**, 1356–1364 (2014)
12. C. Zheng, M.F. Mark, T. Wiegand, S.A. Diaz, J. Cody, F.C. Spano, D.W. McCamant, C.J. Collison, J. Phys. Chem. C **124**, 4032–4043 (2020)
13. C. Zheng, A.R. Penmetcha, B. Cona, S.D. Spencer, B. Zhu, P. Heaphy, J.A. Cody, C.J. Collison, Langmuir **31**, 7717–7726 (2015)
14. K.S. Wilson, A.N. Mapile, C.Y. Wong, Opt. Express **28**, 11339–11355 (2020)
15. K.S. Wilson, Z.S. Walbrun, C.Y. Wong, Spectrochim. Acta A **253**, 119557 (2021)
16. N.J. Hestand, C. Zheng, A.R. Penmetcha, B. Cona, J.A. Cody, F.C. Spano, C.J. Collison, J. Phys. Chem. C **119**, 18964–18974 (2015)
17. H. Yu, M. Fu, Y. Xiao, Phys. Chem. Chem. Phys. **12**, 7386–7391 (2010)